



**Particle Shape Tunes Fragility in Hard Polyhedron Glass-formers**

Journal:	<i>Soft Matter</i>
Manuscript ID	SM-ART-06-2020-001067.R1
Article Type:	Paper
Date Submitted by the Author:	21-Oct-2020
Complete List of Authors:	Teich, Erin; University of Pennsylvania, Bioengineering van Anders, Greg; Queen's University, Physics, Engineering Physics, and Astronomy Glotzer, Sharon; University of Michigan, Chemical Engineering

Cite this: DOI: 00.0000/xxxxxxxxxx

Particle shape tunes fragility in hard polyhedron glass-formers<sup>†</sup>Erin G. Teich,<sup>a‡</sup> Greg van Anders,<sup>abc§</sup> and Sharon C. Glotzer<sup>\*abcd</sup>Received Date  
Accepted Date

DOI: 00.0000/xxxxxxxxxx

We demonstrate that fragility, a technologically relevant characteristic of glass formation, depends on particle shape for glass-formers comprised of hard polyhedral particles. We find that hard polyhedron glass-formers become stronger (less fragile) as particle shape becomes increasingly tetrahedral. We correlate fragility with local structure, and show that stronger systems display a stronger preference for a pairwise face-to-face motif that frustrates global periodic ordering and gives rise in most systems studied to bond angle distributions that are peaked around the ideal tetrahedral bond angle. We demonstrate through mean-field-like simulations of explicit particle pairs and surrounding baths of "ghost" particles that the prevalence of this pairwise configuration can be explained via free volume exchange and emergent entropic force arguments. Our study provides a clear and direct link between the local geometry of fluid structure and the properties of glass formation, independent of interaction potential or other non-geometric tuning parameters. We ultimately demonstrate that the engineering of fragility in colloidal systems via slight changes to particle shape is possible.

## 1 Introduction

The transformation of a fluid to a glass as it is quenched beneath its melting temperature or above its melting density remains yet to be fully elucidated. Numerous theories<sup>1–6</sup> on the thermodynamics and nature of the glass transition compete for dominance within the scientific community. Despite the ongoing debate regarding the underlying physical mechanism of the glass transition, however, glass is a material that has been used for thousands of years<sup>7</sup> to build tools ranging from vessels that carry water to cables that carry light<sup>8</sup>. Increasingly technical applications rely on the phase change between a crystal and quenched disorder for data storage and memory<sup>9,10</sup>. These applications benefit greatly<sup>11</sup> from advances in methods to precisely control glass-former fragility<sup>12</sup>, a quantity that signifies how dramatically systems slow down on approach to the glass transition.

Glass-former fragility has been explored extensively over the last few decades, with most studies agreeing that fragility is related to local structure. Richert and Angell<sup>13</sup> were the first to consider that fragility might be a consequence of changes to local structure, and variation in fragility due to changes in local

structure has been previously studied by means of tuning polydispersity<sup>14–17</sup>, isotropic pairwise potential shape<sup>18–21</sup>, local bond-orientational ordering<sup>22</sup>, particle aspect ratio<sup>23</sup>, and tetrahedrality in a modified Stillinger-Weber potential<sup>17,24</sup>. Recently, we examined in detail the role that local structure plays generally in crystallization avoidance and dynamical arrest in a family of hard-particle glass-formers<sup>25</sup>. In these systems, where thermodynamics away from infinite pressure is dictated by entropy maximization alone, competing local structures exist in glass-formers, with each structure prevalent in crystals assembled by particles of closely-related shapes. Thus, local structural competition prevents these glass-forming systems from crystallizing. Because the origin of this vitrification is due solely to local structural geometry, hard particle systems provide an ideal platform for examining the role of geometry in fragility.

In this paper, using the same family of hard polyhedron glass-formers<sup>25</sup>, we show via equilibrated Monte Carlo simulations that changes to particle shape (and consequently local structure) not only control whether or not glass formation occurs, but also influence glass-former fragility. We find that systems are less fragile as particle shapes become increasingly tetrahedral, although all systems remain in the fragile regime, as is typical for hard particles<sup>26–28</sup>. Increasing tetrahedrality corresponds to an increased preference in the system for facet-aligned pairwise motifs, explored thoroughly in Ref. 25. These motifs are characteristic of the dodecagonal quasicrystal self-assembled from tetrahedra<sup>29–31</sup>. We perform additional simulations of explicit particle pairs in baths of "ghost particles" (that is, particles that cannot overlap with the pair but may overlap with each other) of the same size and shape as the particles comprising the pair, to

<sup>a</sup> Applied Physics Program, University of Michigan, Ann Arbor MI 48109.<sup>b</sup> Department of Physics, University of Michigan, Ann Arbor MI 48109.<sup>c</sup> Department of Chemical Engineering, University of Michigan, Ann Arbor MI 48109.<sup>d</sup> Biointerfaces Institute, University of Michigan, Ann Arbor MI 48109.<sup>†</sup> Electronic Supplementary Information (ESI) available. See DOI: 00.0000/0000000000/<sup>‡</sup> Present address: Department of Bioengineering, University of Pennsylvania, Philadelphia PA 19104.<sup>§</sup> Present address: Department of Physics, Engineering Physics & Astronomy, Queen's University, Kingston ON K7L 3N6.

show that preference for this pairwise configuration can be explained through free volume exchange between a particle pair and a surrounding mean field of particles. Finally, we investigate the three-body structural consequences of this pairwise preference through calculation of triplet bond angle distributions in the equilibrated Monte Carlo simulations. Our results are consistent with theories<sup>32,33</sup> that posit that stronger frustration against periodic ordering results in stronger glass-formers. In contrast to other studies, however, here we demonstrate this connection in a colloidal system of hard particles, permitting a clear demonstration of the link between particle geometry, local structure and glass-forming fragility, independent of interaction potential or other non-geometric parameters. Our results provide guidance on engineering fragility in hard polyhedron systems via changes to particle shape.

## 2 Methods

### 2.1 The 323 shape family

All systems studied in this paper are monatomic and consist of hard, volume-excluding particles culled from a two-parameter family of polyhedra that are interrelated via continuous truncations. This family, the spheric triangle invariant 323 family, contains polyhedra that result from truncating the vertices and/or edges of a tetrahedron at varying radial distances from its center. Densest packings<sup>34</sup>, assembly<sup>35,36</sup> and glassy<sup>25</sup> behavior, and even photonic properties<sup>37</sup> of these systems have been studied elsewhere. Following previous convention<sup>35</sup>, we parameterize edge truncation with  $\alpha_a \in [0, 1]$  and vertex truncation with  $\alpha_c \in [0, 1]$  such that  $(\alpha_a, \alpha_c) = (0, 1)$  and  $(1, 0)$  both denote a tetrahedron,  $(\alpha_a, \alpha_c) = (0, 0)$  denotes an octahedron, and  $(\alpha_a, \alpha_c) = (1, 1)$  denotes a cube. The 323 family is displayed in Fig. 1A, with example polyhedra shown above their location in this shape space. Note that the family is identical under reflection across the line  $\alpha_a = \alpha_c$  due to the symmetry of the tetrahedron.

We focus on the glass-forming behavior of four particle shapes in this family, marked with asterisks in Fig. 1A and shown in Fig. 1B. These shapes, at  $(\alpha_a, \alpha_c) = (0.2, 0.5)$ ,  $(0, 0.5)$ ,  $(0, 0.6)$ , and  $(0, 0.7)$ , showcase differing degrees of tetrahedral truncation. Two of them,  $(\alpha_a, \alpha_c) = (0.2, 0.5)$  and  $(0, 0.5)$ , were previously found not to self-assemble into any crystal structure over a range of densities between  $\phi = 0.5$  and  $\phi = 0.64$ <sup>25</sup>. The others,  $(\alpha_a, \alpha_c) = (0, 0.6)$  and  $(0, 0.7)$ , self-assembled a dodecagonal quasicrystal<sup>29,36,38</sup> at  $\phi = 0.6$  and  $\phi = 0.56$  respectively<sup>25</sup>. In this study, we focus on these systems at densities for which no self-assembly was observed previously, to study their behavior under super-cooled (or more accurately, “super-compressed”) conditions.

### 2.2 Simulations

We performed two types of simulations using the hard particle Monte Carlo (HPMC)<sup>39</sup> extension of the open-source simulation toolkit HOOMD-blue<sup>40,41</sup>. We first used isochoric Monte Carlo sampling of one-component systems with constant maximum move sizes to evaluate dynamical and structural characteristics of each glass-forming system. To perform sampling, random

translations and rotations were attempted and only rejected if they resulted in particle overlaps. Our particular procedure was detailed previously in Ref. 25. For each particle shape, we ran simulations of 4096 particles in which we quenched the system from low densities to final densities between  $\phi = 0.3$  and  $\phi = 0.64$ , equilibrated for approximately 50 million MC sweeps (between 7.8 and 208,000  $\tau_\alpha$ ) at the final density, and then collected structural and dynamical data for approximately 100 million MC sweeps (between 15.6 and 417,000  $\tau_\alpha$ ) at that density. Here,  $\tau_\alpha$  refers to the alpha relaxation time of each system; its calculation is detailed in the next section and reported in the *Results*. Each trajectory length is many times the highest value of  $\tau_\alpha$ , implying that each system is in equilibrium at least with respect to the quantities of interest in this paper, and is thus super-cooled (or in the case of these hard particle systems, “super-compressed”). To perform the quench, we first initialized each system in a sparse cubic array inside a large cubic box with periodic boundary conditions, then randomized it via isochoric MC sampling for 10,000 MC sweeps, and finally rescaled box vectors by a scale factor of 0.9995 until the target density was reached. During equilibration and data collection, maximum rotational and translational move sizes were held fixed at values chosen to most efficiently structurally relax a typical system at  $(\alpha_a, \alpha_c) = (0, 0.5)$ ,  $\phi = 0.6$ . We chose a maximum rotational move size that gives a rotational acceptance ratio of approximately 0.3 in this system at  $\phi = 0.6$ , and a maximum translational move size that results in the smallest relaxation time  $\tau_\alpha$  for this system at  $\phi = 0.6$ , following work done in other Monte Carlo studies of glass-formers<sup>27,42</sup>. The relaxation time was determined through fitting a Kohlrausch-Williams-Watts (KWW)<sup>43,44</sup> function to the real part of the self-intermediate scattering function  $F_s(k, t)$  explained in the next section.

We also performed separate “ghost particle” simulations to isolate the effects of osmotic pressure on particle pairs. Simulations consisted of only two particles in the presence of ghost particles of the same size and shape as the particle pair. In these simulations, we attempted trial moves for each member of the pair, and rejected moves that resulted in any overlaps with a temporary set of ghost particles randomly inserted into the free volume of the old pair configuration. Trial moves were accepted otherwise. Ghost particles are non-interacting with each other and a new set (whose number depended on specified ghost particle volume fraction) was randomly inserted at each trial move, only remaining in memory for the duration of the move. We used the implicit depletion algorithm developed in Ref. 45; further details can be found in that reference. For each particle shape, we performed 10 replicate simulations, each of which swept through increasing ghost particle volume fractions between 0 and 30. Note that since ghost particles do not interact with each other, their volume fraction can be larger than 1. Initially running the simulation at a ghost particle volume fraction of 0, or equivalently without ghost particles, thermalized each system prior to the introduction of ghost particles at volume fractions greater than 0. We collected data for 100,000 MC sweeps at each ghost particle volume fraction, in intervals of 100 MC sweeps. We tuned move sizes during these simulations to maintain move acceptance ratios around 0.2.

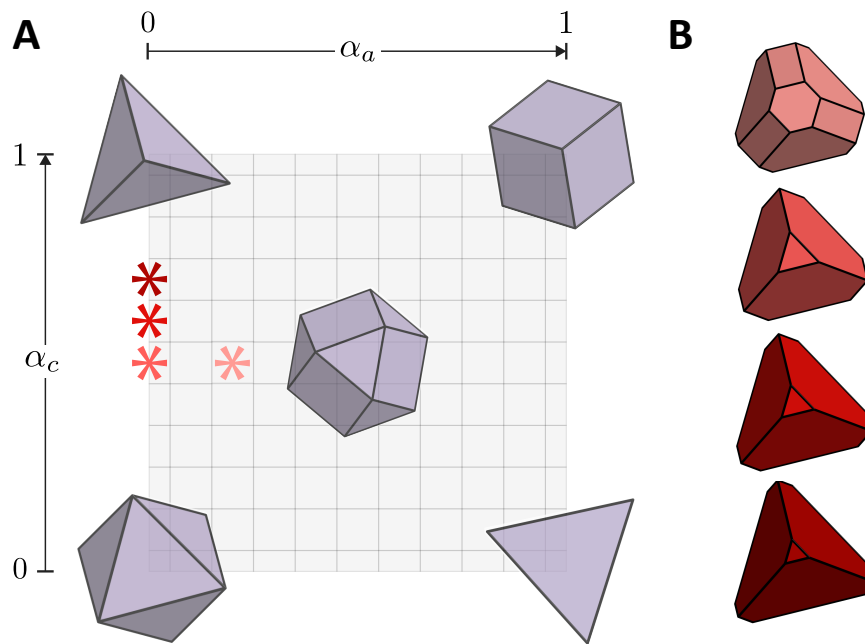


Fig. 1 The systems of interest considered in this study. (A) The 323 shape family, with example polyhedra overlaid above their corresponding locations in shape space. The particle shapes considered in this paper are denoted by asterisks in shape space, and drawn in (B). Colors of each particle shape match the color of the corresponding asterisk in shape space.

### 2.3 Analysis

To characterize dynamics in the four systems studied in this paper, we calculated the mean-squared displacement  $\langle \Delta r^2(t) \rangle$ , the real part of the self-intermediate scattering function  $F_s(k, t)$  (computed at the  $k$  value associated with the first peak of the static structure factor), the non-Gaussian parameter  $\alpha(t)$ <sup>46</sup>, and the self-part of the four-point susceptibility  $\chi_4^{SS}(t)$ <sup>47</sup>. The dynamics of two of these systems,  $(\alpha_a, \alpha_c) = (0.2, 0.5)$  and  $(0, 0.5)$ , were studied already in our previous work<sup>25</sup>; plots associated with these systems are reproduced from Fig. 2 of that paper. For all systems, we broke each 100 million MC sweep trajectory into 10 windows of 10 million MC sweeps each, since alpha relaxation in all systems occurred within 10 million MC sweeps. We then took appropriate ensemble averages of all dynamical order parameters over these windows. Error bars were determined through either error propagation or jackknife resampling. The specifics of these parameters and determination of their errors are thoroughly detailed in Sections I.C and I.D of the *Supplementary Information* for Ref. 25, and we refer the interested reader to that resource.

We calculated relaxation times  $\tau_\alpha$  (and their associated error bars) directly from the data by taking the mean (and standard error of the mean) of all values  $\{t\}$  for which  $|\text{Re}F_s(k, t) - \text{Re}F_s(k, 0)|/e < \Delta$ , where  $\text{Re}F_s(k, t)$  is the real part of the self-intermediate scattering function and  $\Delta$  is a tolerance chosen from the set  $\{0.01, 0.05, 0.1\}$ . We chose the  $\Delta$  value that gave a relaxation time  $\tau_\alpha$  that produced the best fit of  $\text{Re}F_s(k, t)$  to a Kohlrausch-Williams-Watts (KWW)<sup>43,44</sup> stretched exponential functional form,  $B \exp[-(t/\tau_\alpha)^\beta]$ , at all densities. We varied  $B$  and  $\beta$  as fitting parameters. Further detail regarding the fitting procedure, as well as the fits themselves, can be found in the *Sup-*

*plementary Information*.

For each system, we scaled density by the factor  $\phi_C$  and relaxation time by the factor  $\kappa$  to facilitate comparison of their relaxation times on a single plot. Density scaling accounts for possible variation in the onset of the glass transition among systems, while relaxation time scaling accounts for the different length scales (and thus different values of  $k$  – corresponding to the first peak of the static structure factor – used to calculate the self-intermediate scattering function and consequent relaxation time) associated with each particle shape.  $\kappa$  is defined for each system by  $\kappa^{-1} = \tau_\alpha(\phi = 0.3)$ . This scaling collapses the data for small  $\phi$ . Similar scaling has been performed elsewhere<sup>27,48,49</sup>.  $\phi_C$  is defined for each system as the density at which  $\tau_\alpha^{VFT}(\phi_C) = 2$  million MC sweeps.  $\tau_\alpha^{VFT}(\phi)$  is the extrapolation of  $\tau_\alpha$  according to its fit by a modified Vogel-Fulcher-Tammann (VFT) functional form<sup>50</sup>:

$$\tau_\alpha^{VFT}(\phi) = \tau_\infty \exp \left[ \frac{A}{(\phi_0 - \phi)^\delta} \right] \quad (1)$$

We used  $\delta = 2$  because this form has been found to accurately model relaxation times in other hard particle systems at high density<sup>27,48,51</sup>.

We quantified the fragility of each system by calculating the slope  $s(\phi/\phi_C) \equiv \partial \log \tau_\alpha / \partial (\phi/\phi_C)$  directly from the relaxation time data, rather than relying on any fits to this data. To calculate this derivative at each value of  $\phi/\phi_C$ , we used second-order accurate central differences for interior values of  $\phi/\phi_C$  and first-order accurate differences at the boundary values of  $\phi/\phi_C$  via NumPy's `gradient` method<sup>52</sup>. We calculated the error associated

with each slope by propagation of the errors associated with each relaxation time. Specifically, we calculated the variance of each slope as a first-order Taylor series expansion of the variances of the relaxation times used to calculate that slope according to the appropriate difference formula.

The glass transition limit of the slope  $s(\phi/\phi_C)$  is known as the “fragility”<sup>53</sup> or “steepness index”<sup>54</sup>. This parameter, denoted by  $m$  in the literature, defines the slope of the (usually extrapolated) relaxation curve at the glass transition, and is larger for more fragile glass-formers. However, we have chosen to report the numerical derivative  $s(\phi/\phi_C)$  at all densities, rather than the single scalar  $m$ , to indicate the relaxation behavior of our systems on approach to the glass transition. As  $\phi$  increases, there is a  $\phi$  regime in which a more fragile glass-former’s slope  $s(\phi/\phi_C)$  is larger than the slope for a less fragile glass-former. Our choice is maximally transparent, and most importantly, does not rely explicitly on any fits to theoretical models. Our goal is not to locate the exact glass transitions of our systems, but instead to investigate relative differences in fragility on approach to the glass transition as particle shape is changed.

## 3 Results and Discussion

### 3.1 Glassy dynamics

Fig. 2 shows four order parameters that characterize dynamics associated with glass formation, each calculated for the four systems studied in this paper at a variety of densities. We find that all quantities behave as expected for a fluid or liquid approaching the glass transition. The top two rows of Fig. 2 show  $\langle \Delta r^2(t) \rangle$  and  $\text{Re}[F_s(k, t)]$ , where we set  $k$  to be the value associated with the first peak of the static structure factor for each system. Static structure factors are shown in the *Supplementary Information*. For all systems, plateaus develop in these parameters at intermediate times and high densities, and plateaus persist for longer times as density increases. These plateaus indicate caging in the system, when particles on average are trapped by their surrounding neighbors, and dynamics slow. Only at later times do particles escape these cages, and dynamics become diffusive. The bottom two rows of Fig. 2 show  $\alpha(t)$  and  $\chi_4^{\text{SS}}(t)$ . Peaks in these parameters generally develop at later times and grow in height as density increases. The time at which each peak occurs also matches, to eye, the transition from a caged regime to a diffusive regime in the corresponding  $\langle \Delta r^2(t) \rangle$  and  $\text{Re}[F_s(k, t)]$  signatures. Peaks in  $\alpha(t)$  and  $\chi_4^{\text{SS}}(t)$  indicate dynamical heterogeneity in the system; that these parameters reach their maxima around the time when  $\langle \Delta r^2(t) \rangle$  and  $\text{Re}[F_s(k, t)]$  show a transition from a caged regime to a diffusive regime implies that the relaxation events associated with cage escape are dynamically heterogeneous, in agreement with behavior reported in many other glass-formers<sup>55–60</sup>. Previous works have indicated that relaxation proceeds via cooperative rearrangement<sup>57,58,61,62</sup>. We leave a more detailed study of spatially heterogeneous dynamics in these systems to future work.

We note that the increase in  $\alpha(t)$  as  $t \rightarrow 0$  at short times is due to the discrete nature of Monte Carlo sampling; this behavior is in contrast to that for systems simulated via molecular dynamics (for which  $\alpha(t) \rightarrow 0$  as  $t \rightarrow 0$ , see e.g. 57,63) and may appear

unusual at first glance. We refer the interested reader to Ref. 25 for more detail regarding this point.

### 3.2 Fragility

Fig. 3A shows relaxation time  $\tau_\alpha$  for the four systems examined in this paper. Error bars indicate standard deviations of the mean, and are smaller than the marker size. Lines in Fig. 3A are VFT fits to the relaxation data (see the *Methods* section for more detail). For some systems, relaxation times at high  $\phi$  fall off the trend lines established by the VFT fits, in agreement with relaxation times observed in systems of hard tetrahedra in Ref. 27. The authors of that paper hypothesized that this deviation from the VFT fit was due to higher order local structure formation in systems of tetrahedra at high density. We do not speculate on the cause of this peculiar behavior here, but merely note that as a result of this behavior, we did not include some values of  $\tau_\alpha$  at high  $\phi$  when fitting the VFT functional form to our data. Were we to include those values, the accuracy of the VFT fits would be greatly reduced. Solid lines in the figure pass through the data points that were actually fit, and dotted lines indicate continuations of the fit function.

Fig. 3B shows scaled relaxation time as a function of scaled density for our sample systems (see the *Methods* section for more detail). Error bars for each scaled relaxation time are the appropriately scaled standard deviations of the mean, and remain smaller than the marker size. Relaxation times for each particle shape show different slopes (plotted in Fig. 3C as  $s(\phi/\phi_C)$ ) on approach to the glass transition, and thus different fragilities. Error bars are smaller than marker sizes, and were determined as detailed in the *Methods* section. Fig. 3C shows generally that, as particle shape increases in tetrahedrality,  $s(\phi/\phi_C)$  is smaller in the high density regime. Thus, particle shapes with increasing tetrahedrality are less fragile. Crucially, these systems’ drop in  $s(\phi/\phi_C)$  occurs in the density regime for which their  $\tau_\alpha$  values fall below the VFT fits, as mentioned previously and shown inset in Fig. 3B. This apparent decrease in fragility at high density is reminiscent of the fragile-to-strong crossover<sup>64</sup> seen in molecular tetrahedral systems at low temperature, including silicon<sup>65</sup>, silica<sup>66</sup>, water<sup>67</sup>, and confined water<sup>68</sup>. We do not have adequate data to support claims of a similar crossover in our systems, so we must instead conservatively say that all of our systems are fragile, but that some are less fragile than others. The connection to the fragile-to-strong crossover remains intriguing, however, and emphasizes regardless the importance of determining fragility directly from the data in our systems, rather than relying on VFT fitting procedures. Our result, that systems are less fragile as their constituent particle shapes are increasingly tetrahedral, is consistent with others<sup>18,20</sup> that show a decrease in fragility with an increase in some aspect of tetrahedrality in the system. It also tracks with the more general common knowledge that tetrahedral network glass-formers are strongest<sup>69</sup>. We note, however, that all systems studied here are fragile glass-formers; each system’s growth in relaxation time is super-Arrhenius over the entire density range shown. Indeed, systems of hard particles of varying shapes, experimental or computational, typically exhibit fragile

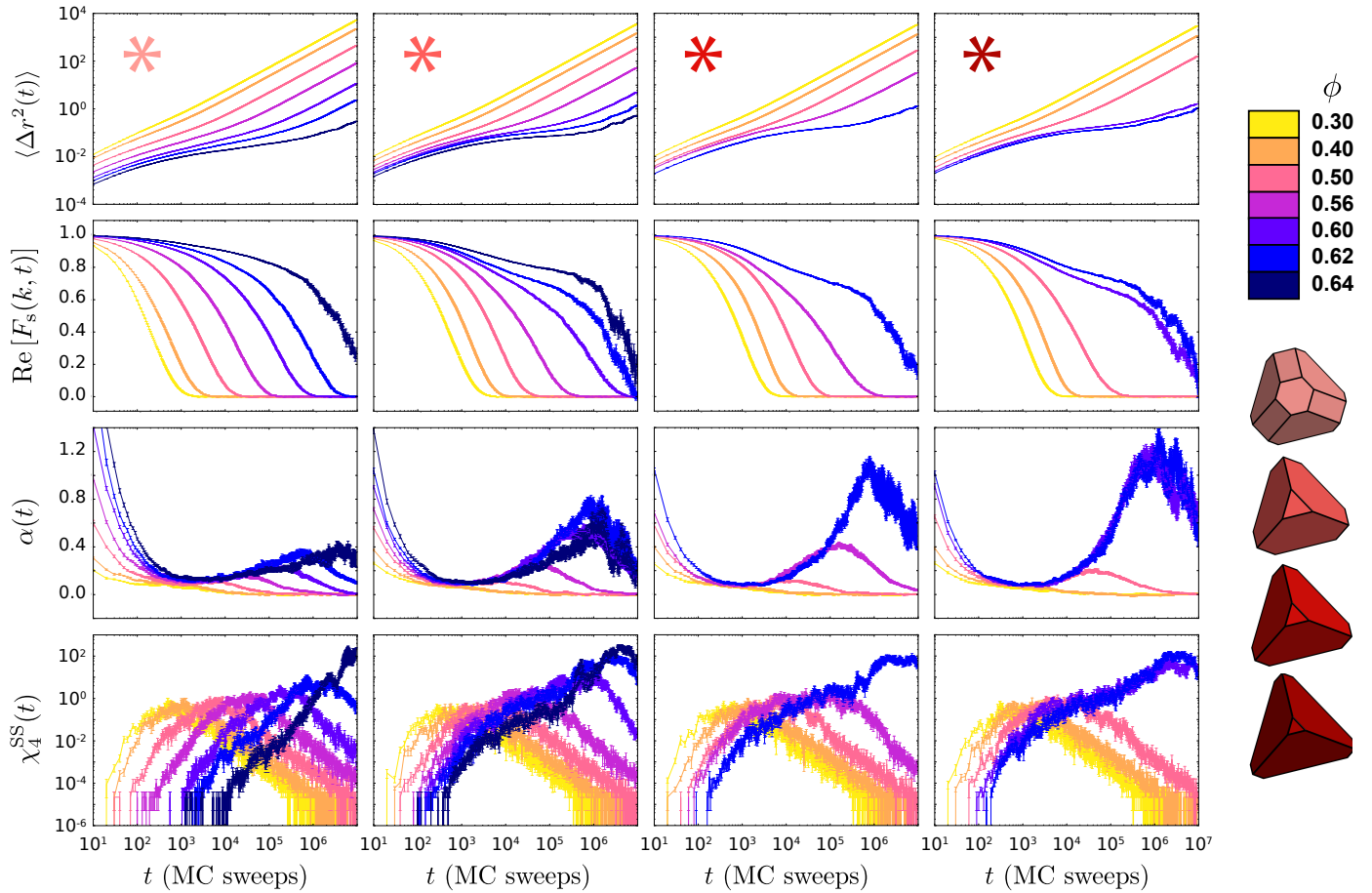


Fig. 2 The mean-squared displacement  $\langle \Delta r^2(t) \rangle$ , the real part of the self-intermediate scattering function  $F_s(k, t)$ , the non-Gaussian parameter  $\alpha(t)$ , and the four-point susceptibility  $\chi_4^{SS}(t)$ , measured at a variety of densities for the indicated state points in our shape space. Signatures in all four order parameters indicate that these systems are glass-formers. The increase in  $\alpha(t)$  as  $t \rightarrow 0$  is due to the discrete nature of our Monte Carlo sampling.

behavior<sup>26,28</sup>, and super-Arrhenius relaxation behavior was also observed in a system of hard non-truncated tetrahedra studied elsewhere<sup>27</sup>.

For completeness, we tabulate parameters associated with VFT fits to our data in the *Supplementary Information*. However, we note that due to the aforementioned discrepancies in  $\tau_\alpha$  at high  $\phi$  and our consequent *ad hoc* fitting procedure, these values may not be especially informative.

Finally, we note that we have used  $\phi$  as the control parameter to indicate approach to the glass transition, in deference to standards established by a wealth of literature on hard particle glasses – including hard anisotropic ellipsoid and dimer particle glasses<sup>23,28,70–72</sup> – and due to the experimental accessibility of volume fraction. However, recent work<sup>51</sup> argues that the relevant control parameter in hard particle systems is reduced pressure (or compressibility factor) rather than density. We include an analysis of our systems using reduced pressure rather than density in the *Supplementary Information*. Curiously, because of these systems' different particle shapes and thus different dependencies of reduced pressure on density, Angell plots of  $\tau_\alpha$  with respect to pressure look very different than those shown in Fig. 3B. Indeed, systems of hard polyhedra of various geometries are known to have varying equations of state<sup>73</sup>. As far as we know, our observation of a qualitative difference in a multi-system Angell plot as a function of pressure rather than density, a consequence of the systems' differing equations of state, is the first reported for systems of hard anisotropic particles. The only other instance of this phenomenon of which we are aware occurs for isotropic spheres; in this case, curves of  $\tau_\alpha$  for systems of varying polydispersity collapse when plotted against the compressibility factor  $Z$ , but do not collapse when plotted against the density<sup>74</sup>. In our case, by contrast, the shapes of the  $\tau_\alpha$  curves for different particle shapes change when plotted against compressibility factor  $Z$  rather than density, and collapse does not happen. Nevertheless, our general finding that more tetrahedral particles are less fragile at high densities (or high pressures) still holds, since these systems still have smaller-than-expected relaxation times (with respect to a VFT extrapolation) in the high pressure regime.

### 3.3 Local pairwise structure

To explicitly correlate structure and dynamics on approach to the glass transition, we investigated local structure in our systems. We first considered pairwise structural motifs, or arrangements of every particle with respect to its nearest neighbor. In previous work<sup>25</sup>, we found that competition in pairwise structures prevents crystallization and facilitates dynamical arrest. One of these competing local structures, which we termed the “aligned” motif, consists of two truncated tetrahedra that are face-to-face such that their (truncated) vertices are aligned with each other. An example of this arrangement is shown in the inset of Fig. 3D. We found that this motif is dominant<sup>25</sup> in the dodecagonal quasicrystal that self-assembles from particles that are close to the tetrahedron in shape space<sup>29–31,36,38</sup>.

Here we find that this motif becomes more prevalent as density (and relaxation time) increases in all four systems considered in

this paper. Less fragile glass-formers with increasingly tetrahedral constituent particle shape are increasingly dominated by particle pairs in the aligned configuration at all densities. Regardless of fragility, the fraction of particles participating in the aligned motif increases as relaxation time increases, although less drastically for the more fragile systems due to the presence of other pairwise motifs. Fig. 3D shows these trends. It displays the fraction of aligned pairwise motifs in each system as a function of density scaled by  $\phi_c$ . Aligned motifs were identified by their connection type (face-to-face) and relative rigid body misorientation ( $\theta \sim 70^\circ$ ); further detail can be found in Ref. 25. Aligned motif fractions were calculated in frames separated by 1 million MC sweeps. Motif fractions were collected over groups of 10 frames each, and the mean values are plotted in Fig. 3D with error bars associated with the standard deviation of the mean. Error bars are smaller than marker sizes in all cases.

### 3.4 Preferred pairwise configurations due to free volume exchange in a mean field

To further explore the observed preference for the pairwise aligned motif at increasing density and particle tetrahedrality in our systems, we performed simulations of only two particles in the presence of ghost particles of the same size and shape as the particle pair. Simulation details can be found in the *Methods* section. These simulations represent reduced systems that isolate the local packing preferences for only a pair of particles with respect to a surrounding mean field of particles. At a specified ghost particle volume fraction, the simulations agnostically produce pairwise particle configurations that maximize system entropy as mediated by free volume exchange between the pair and the surrounding bath of ghost particles. This is in contrast to the other hard particle Monte Carlo simulations reported in this work, in which all particles are explicit and local packing preferences of groups of more than two particles may influence local structure and global behavior.

We find that the aligned pairwise motif emerges in these simulations, and its emergence behaves qualitatively similarly to the emergence of the aligned pairwise motif in our full glass-former simulations: aligned pairwise motif prevalence increases with increasing ghost particle density and increasing particle tetrahedrality. Fig. 4 shows these results: for each particle shape at varying ghost particle volume fractions, we plot the fraction of pair members observed to adopt the aligned motif with their neighbor. To calculate these fractions, we identified whether each pair member adopted the aligned motif with its neighbor in each simulation snapshot at a particular ghost particle volume fraction, then computed the fraction of aligned motif instances over all pair members and all snapshots. We then averaged aligned motif fraction over all replicate simulations at each ghost particle volume fraction. Error bars show the standard deviation over all replicates.

Our results suggest two conclusions. The first is that the consideration of pairwise interactions in a mean field of surrounding particles, as theoretically explored by van Anders et al.<sup>75</sup>, is enough to explain the local structure of our hard particle systems even though higher-order interactions may be present in the sys-

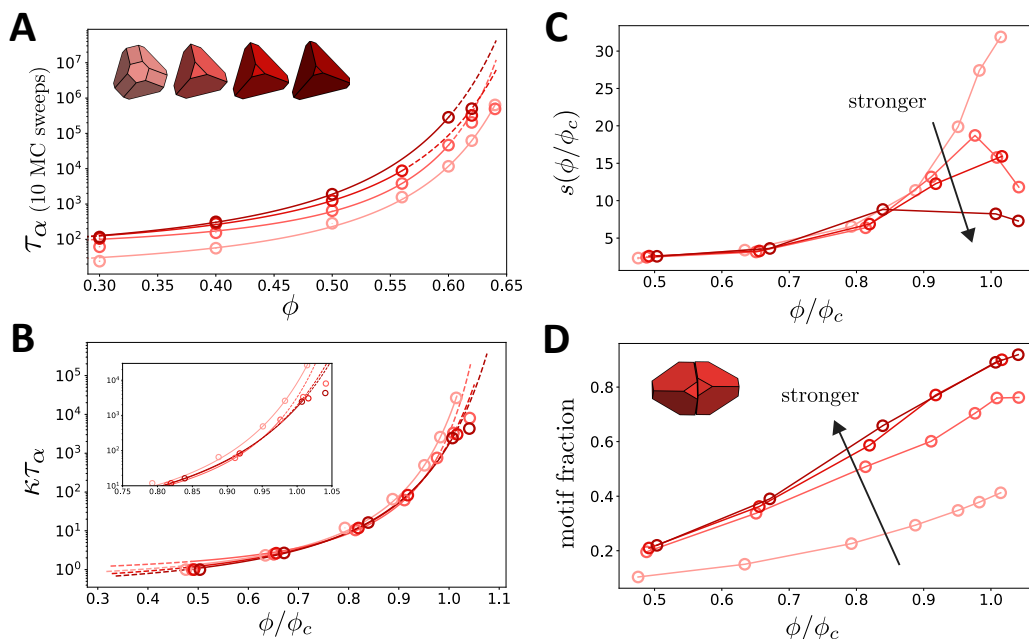


Fig. 3 Glass-forming systems exhibit a range of fragilities, with systems becoming “stronger” (less fragile) as particle shapes become increasingly tetrahedral, indicated by increasingly red color. (A) An Angell plot of relaxation time as a function of density. Relaxation time is in units of 10 MC sweeps. Lines through the data points are VFT fits to relaxation time. Error bars are smaller than the marker size. (B) A scaled Angell plot, where density is scaled by  $\phi_c$  and relaxation time is scaled by  $\kappa$ , both defined in the main text. Error bars are scaled appropriately and remain smaller than the marker size. Inset is a zoom of the same plot at high density, showing that measured relaxation times in several systems fall well below the extrapolated VFT fit. (C) Slope of the log of relaxation time,  $s(\phi/\phi_c) \equiv \partial \log \tau_\alpha / \partial (\phi/\phi_c)$ , as a function of scaled density. Systems of more tetrahedral particle shapes tend to be stronger. Error bars are smaller than the marker size. (D) Fractions of particles in the aligned pairwise motif as a function of scaled density. An example of this motif for the particle shape  $(\alpha_a, \alpha_c) = (0, 0.5)$  is inset. Error bars are smaller than the marker size.

tem. The second is that tetrahedral particles adopt the aligned motif at high enough volume fraction because this pairwise configuration gives more free volume to the surrounding particle bath than any other pairwise arrangement, and as particles become increasingly tetrahedral, the free volume advantage of the aligned motif only increases. Thus, as particles increase in tetrahedrality, they are more likely to adopt the aligned motif at lower volume fractions. Emergent entropic forces in the system, in other words, increasingly bias pairs of particles towards the aligned configuration as particles increase in tetrahedrality.

### 3.5 Higher-order structure

We additionally investigated the higher-order structural implications of preferred pairwise configurations in our systems. We measured bond angle distributions to examine three-body structural signatures and to place our work in the context of other computational studies of quenched liquids of varying tetrahedral bond strength and flexibility<sup>17,24,76–79</sup>. Some of these studies<sup>76,78,79</sup> used distributions of triplet bond angles to demonstrate the structural effects of changes to imposed bond strength or flexibility: they found that as tetrahedral bond strength increases or bond flexibility decreases, triplet bond angle distributions become increasingly peaked around the ideal tetrahedral angle  $\sim 109.5^\circ$ .

Our results, shown in Fig. 5, are in general agreement with that result. We found the nearest four neighbors of each particle in our systems, then calculated bond angles between that particle and all possible two-neighbor subsets. We define bond angle to be

the angle between the vectors pointing from the center of mass of the particle to the centers of mass of its two specified neighbors. We accumulated histograms of bond angles over windows of 10 frames separated by 1 million MC sweeps, then ensemble-averaged these histogram bin values over 10 such windows in each trajectory. Error bars are standard deviations of the mean.

We will address the behaviors of the system at  $(\alpha_a, \alpha_c) = (0.2, 0.5)$  and the systems with no edge truncation at  $(\alpha_a, \alpha_c) = (0, 0.5)$ ,  $(0, 0.6)$ , and  $(0, 0.7)$  separately. For the systems with no edge truncation, we see an increasing peak around the ideal tetrahedral angle  $\sim 109.5^\circ$  (shown as a dotted vertical line in Fig. 5) with increasing density and as particle shape becomes increasingly tetrahedral, from  $(\alpha_a, \alpha_c) = (0, 0.5)$  to  $(0, 0.7)$ . Effects due to subtle changes in particle shape are subtle, but they can especially be seen for packing fractions below  $\phi = 0.62$ . To quantify these effects, we calculated the full width at half-maximum (FWHM) of the bond angle distributions for  $(\alpha_a, \alpha_c) = (0, 0.5)$ ,  $(0, 0.6)$ , and  $(0, 0.7)$  at all measured values of  $\phi$ . Bond angle FWHM values are shown in the *Supplementary Information*. We find that the bond angle FWHM decreases with increasing density, and is lower for more tetrahedral particles at almost all measured values of  $\phi$ . The behavior of the tetrahedral bond angle peak as a function of density and particle shape tracks the behavior of the aligned pairwise motif fraction, shown in Fig. 3D; thus, it seems that the aligned pairwise motif is an indicator of tetrahedral network structure at least on a three-body level. The small peak around  $45^\circ$  that remains consistently present at densities  $\phi \geq 0.5$ , upon inspection by

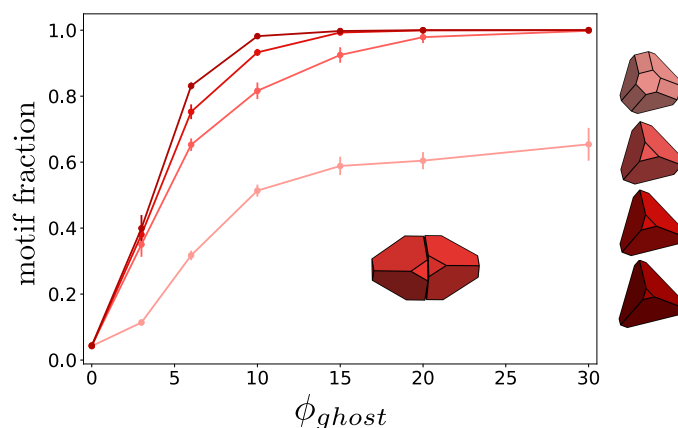


Fig. 4 Results of ghost particle simulations of particle pairs, showing that as particle shape becomes increasingly tetrahedral and as ghost particle density grows, particle pairs are more often in the aligned configuration. Aligned motif fraction is plotted as a function of ghost particle density for all particle shapes, drawn in corresponding colors to the right of the plot. The inset shows an example of the aligned pairwise motif. Error bars were calculated at all ghost particle densities via methods explained in the main text.

eye, seems to indicate the acute bond angle between one tetrahedron and two of its neighbors that are aligned face-to-face with each other. An example snapshot of this type of motif is shown in the *Supplementary Information*.

The bond angle distribution for  $(\alpha_a, \alpha_c) = (0.2, 0.5)$  becomes increasingly bimodal with increasing density: its peak at  $\sim 116.6^\circ$  (consistent with an icosahedral local environment) remains consistent with increasing density, while its other peak moves from  $\sim 63.4^\circ$  (also consistent with an icosahedral local environment) at the lowest density shown to  $\sim 70.9^\circ$  at the highest density shown. These peaks are distributed over bond angle values closer to those found in the close-packed structures of *bcc*, *fcc*, and  $\gamma$ -brass. Bond angles for these crystals are calculated and shown in the *Supplementary Information*, along with a plot showing the bond angle distributions for  $(\alpha_a, \alpha_c) = (0.2, 0.5)$  at all densities simultaneously. In Ref. 25, we found that the glass-former at  $(\alpha_a, \alpha_c) = (0.2, 0.5)$ , close in shape space to systems that crystallize into *bcc*, *fcc*, and  $\gamma$ -brass, contains pairwise motifs from some of those structures. Thus, the similarity found in this work between the glass-former and these crystals on a three-body structural level seems reasonable.

### 3.6 Frustration

A periodic crystal consisting of all particles forming aligned pairwise motifs with each of their tetrahedrally coordinated neighbors is impossible due to the frustration inherent in perfect polytetrahedral ordering<sup>80</sup>; thus, the aligned motif is indicative of a locally preferred structure that globally frustrates against periodic ordering, but may give rise to quasiperiodic ordering (in the form of a dodecagonal quasicrystal) when higher-order rearrangements of groups of face-to-face aligned particles occur<sup>29</sup>. We find that systems become less fragile as frustration against periodic ordering increases, in agreement with results<sup>14,15,22</sup> supporting a crystallization/frustration competition theory<sup>32,33</sup>. Our study puts this idea into a concrete, geometrical context: systems of hard polyhedra grow less fragile as they move closer to the tetrahedron in

shape space.

## 4 Conclusions

We have shown that hard polyhedral glass-formers with particle shapes culled from a two-dimensional shape space have glass-forming properties that are related to and dependent upon their position in this space. We found a range of fragilities over a small range of particle shapes related to the regular tetrahedron. Stronger (*i.e.* less fragile) glass-formers result when particle shape is less truncated and thus more tetrahedral. We emphasize, however, that all systems remain in the fragile regime, as is expected for hard particles.

We took advantage of the purely geometric nature of our hard particle model to isolate the influence of local structure on system fragility, and found that glass-forming strength corresponds to an increased preference for a pairwise aligned motif—locally preferred but globally impossible—at all densities. Via simulations of explicit pairs of particles surrounded by a field of ghost particles, we verified that this preference for the aligned motif could be explained by considering free volume exchange between particle pairs and a surrounding mean particle field. We also investigated three-body structural effects in our systems via the calculation of triplet bond angles, and found that systems with only vertex truncation show a more pronounced peak around the tetrahedral bond angle with increasing prevalence of the aligned pairwise motif. The system with both edge and vertex truncation contains bond angles more associated with close-packed structures at all densities.

We note that in this paper we have focused on translational relaxation only, and left the study of rotational relaxation in these systems to future work. Investigations regarding rotational relaxation and its relationship to translational relaxation are numerous in molecular<sup>81</sup> and colloidal<sup>82</sup> systems, and a recent study found an apparent orientational glass transition in a plastic crystal consisting of hard polyhedral particles<sup>83</sup>. We look forward to studying in the future the relationship between rotational and

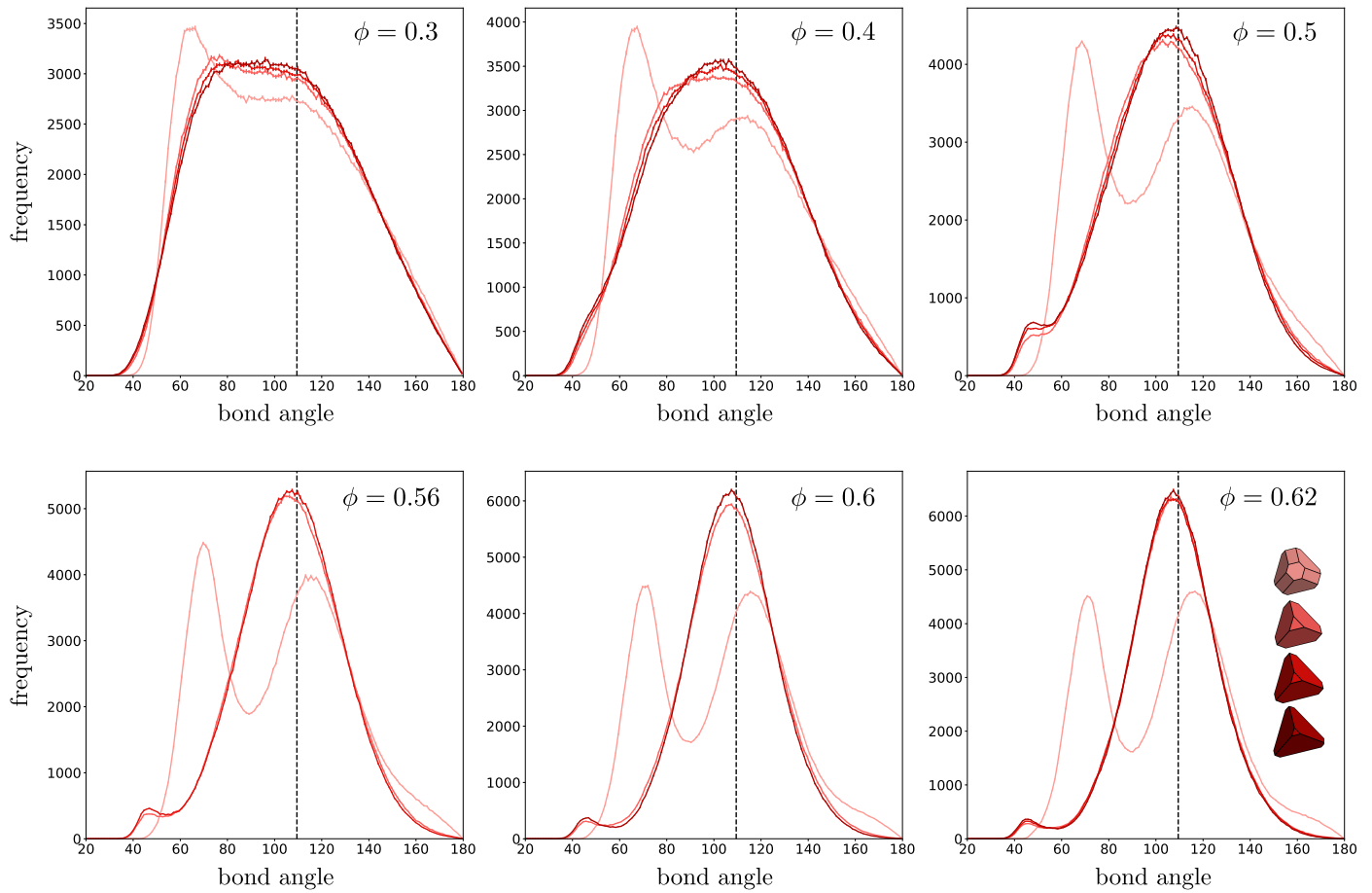


Fig. 5 Bond angle distributions for the four particle shapes studied in this paper and drawn in the lower right plot. Distributions for all particle shapes at varying densities are overlaid in each plot, with the density specified in the upper right corner. Colors of the distributions identify the particle shape of each system. Error bars were calculated via methods defined in the main text. The ideal tetrahedral bond angle,  $\sim 109.5^\circ$ , is drawn as a dotted line in each plot. For the particle shapes with vertex truncation only, peaks around the ideal tetrahedral angle become more pronounced with increasing density and as particle shape becomes more tetrahedral. For the particle shape with edge and vertex truncation, bond angles more closely match those found in close-packed structures.

translational relaxation in the hard particle systems investigated in our paper.

In sum, we have demonstrated a new means of tuning fragility via the tuning of particle shape and consequent local structure. We have found, in agreement with other studies<sup>32,33</sup>, that stronger frustration against periodic ordering results in stronger (less fragile) glass-formers. The truncated tetrahedral particle shapes we have investigated are accessible experimentally<sup>84,85</sup>, in addition to a host of other polyhedral nanoparticle geometries<sup>86</sup>. Truncated tetrahedral nanoparticles, in particular, were found to self-assemble into quasicrystalline<sup>84</sup> and other superstructures<sup>85</sup> also characterized by preferred face-to-face alignment; thus our work may help guide the engineering of glass-formers in related experimental systems. More broadly, our results represent a link between pure geometry and fragility, and thus our conclusions may apply generically to systems in which more complicated interaction potentials or other non-geometric considerations might otherwise obscure the physics governing glass-former fragility, such as chalcogenide compounds whose heat-induced switching between amorphous and crystalline phases enables phase-change memory devices<sup>9,10</sup> and is affected by system fragility<sup>11</sup>.

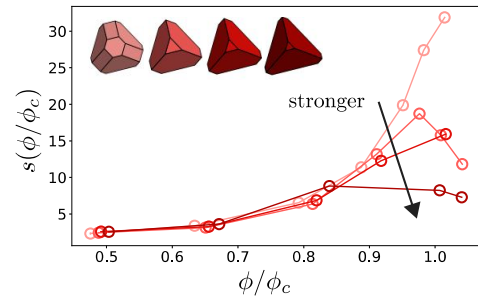
## Acknowledgements

We thank D. Klotsa for sharing her shape space assembly landscapes with us prior to publication of Ref. 36. This research was partially supported by a Simons Investigator award from the Simons Foundation to S.C.G. E.G.T acknowledges support from the National Science Foundation Graduate Research Fellowship Grant DGE 1256260 and a Blue Waters Graduate Fellowship. This research is part of the Blue Waters sustained petascale computing project, which is supported by the National Science Foundation (awards OCI-0725070 and ACI-1238993) and the state of Illinois. Blue Waters is a joint effort of the University of Illinois at Urbana-Champaign and its National Center for Supercomputing Applications. This research also utilized computational resources and services supported by Advanced Research Computing at the University of Michigan, Ann Arbor, and resources provided by the Extreme Science and Engineering Discovery Environment (XSEDE), which is supported by National Science Foundation Grant ACI-1053575, XSEDE Award DMR 140129.

## Notes and references

- 1 G. Adam and J. H. Gibbs, *J. Chem. Phys.*, 1965, **43**, 139–146.
- 2 V. Lubchenko and P. G. Wolynes, *Annual Review of Physical Chemistry*, 2007, **58**, 235–266.
- 3 G. Tarjus, S. A. Kivelson, Z. Nussinov and P. Viot, *Journal of Physics: Condensed Matter*, 2005, **17**, R1143–R1182.
- 4 H. Tanaka, *Journal of Non-Crystalline Solids*, 2005, **351**, 3371–3384.
- 5 D. Chandler and J. P. Garrahan, *Annual Review of Physical Chemistry*, 2010, **61**, 191–217.
- 6 W. Gotze, *Complex Dynamics of Glass-Forming Liquids: A Mode-Coupling Theory*, Oxford University Press, 2009.
- 7 H. Tait, *Five Thousand Years of Glass*, Published for the Trustees of the British Museum by British Museum Press, 1991.
- 8 F. Mitschke, *Fiber Optics: Physics and Technology*, Springer Berlin Heidelberg, 2016.
- 9 M. Wuttig, *Nature Materials*, 2005, **4**, 265–266.
- 10 M. Wuttig and N. Yamada, *Nature Materials*, 2007, **6**, 824–832.
- 11 W. Zhang, R. Mazzarello, M. Wuttig and E. Ma, *Nature Reviews Materials*, 2019, **4**, 150–168.
- 12 C. A. Angell, *Science*, 1995, **267**, 1924–1935.
- 13 R. Richert and C. A. Angell, *The Journal of Chemical Physics*, 1998, **108**, 9016–9026.
- 14 T. Kawasaki, T. Araki and H. Tanaka, *Physical Review Letters*, 2007, **99**, 215701.
- 15 T. Kawasaki and H. Tanaka, *Journal of Physics: Condensed Matter*, 2010, **22**, 232102.
- 16 R. Kurita and E. R. Weeks, *Physical Review E*, 2010, **82**, 041402.
- 17 J. Russo, F. Romano and H. Tanaka, *Physical Review X*, 2018, **8**, 021040.
- 18 P. Jund, M. Rarivomanantsoa and R. Jullien, *J. Phys.-Cond. Matt.*, 2000, **12**, 8777–8784.
- 19 D. Coslovich and G. Pastore, *Journal of Chemical Physics*, 2007, **127**, year.
- 20 M. Ozawa, K. Kim and K. Miyazaki, *J. Stat. Mech.: Theor. Exp.*, 2016, **2016**, 074002.
- 21 C. E. Pueblo, M. Sun and K. F. Kelton, *Nature Materials*, 2017, **16**, 792–796.
- 22 H. Shintani and H. Tanaka, *Nature Physics*, 2006, **2**, 200–206.
- 23 T. Shen, C. Schreck, B. Chakraborty, D. E. Freed and C. S. O'Hern, *Physical Review E*, 2012, **86**, 1–9.
- 24 V. Molinero, S. Sastry and C. A. Angell, *Physical Review Letters*, 2006, **97**, 075701.
- 25 E. G. Teich, G. van Anders and S. C. Glotzer, *Nature Communications*, 2019, **10**, 64.
- 26 G. L. Hunter and E. R. Weeks, *Reports on Progress in Physics*, 2012, **75**, year.
- 27 N. Tasios, A. P. Gantapara and M. Dijkstra, *Journal of Chemical Physics*, 2014, **141**, year.
- 28 Z. Zheng, R. Ni, F. Wang, M. Dijkstra, Y. Wang and Y. Han, *Nature Communications*, 2014, **5**, 1–12.
- 29 A. Haji-Akbari, M. Engel, A. S. Keys, X. Zheng, R. G. Petschek, P. Palffy-Muhoray and S. C. Glotzer, *Nature*, 2009, **462**, 773–777.
- 30 A. Haji-Akbari, M. Engel and S. C. Glotzer, *Journal of Chemical Physics*, 2011, **135**, year.
- 31 A. Haji-Akbari, M. Engel and S. C. Glotzer, *Physical Review Letters*, 2011, **107**, 1–5.
- 32 H. Tanaka, *Journal of Non-Crystalline Solids*, 2005, **351**, 678–690.
- 33 H. Tanaka, *The European Physical Journal E*, 2012, **35**, 113.
- 34 E. R. Chen, D. Klotsa, M. Engel, P. F. Damasceno and S. C. Glotzer, *Physical Review X*, 2014, **4**, 011024.
- 35 C. X. Du, G. van Anders, R. S. Newman and S. C. Glotzer,

- Proceedings of the National Academy of Sciences*, 2017, **114**, E3892–E3899.
- 36 D. Klotsa, E. R. Chen, M. Engel and S. C. Glotzer, *Soft Matter*, 2018, **14**, 8675–8862.
- 37 R. K. Cersonsky, J. Dshemuchadse, J. Antonaglia, G. van Anders and S. C. Glotzer, *Physical Review Materials*, 2018, **2**, 125201.
- 38 P. F. Damasceno, M. Engel and S. C. Glotzer, *ACS Nano*, 2012, **6**, 609–614.
- 39 J. A. Anderson, M. Eric Irrgang and S. C. Glotzer, *Computer Physics Communications*, 2015, **204**, 21–30.
- 40 J. Anderson, C. Lorenz and A. Travasset, *Journal of Computational Physics*, 2008, **227**, 5342–5359.
- 41 J. Glaser, T. D. Nguyen, J. A. Anderson, P. Lui, F. Spiga, J. A. Millan, D. C. Morse and S. C. Glotzer, *Computer Physics Communications*, 2015, **192**, 97–107.
- 42 L. Berthier and W. Kob, *Journal of Physics: Condensed Matter*, 2007, **19**, 205130.
- 43 R. Kohlrausch, *Annalen der Physik und Chemie*, 1854, **167**, 179–214.
- 44 G. Williams and D. C. Watts, *Transactions of the Faraday Society*, 1970, **66**, 80.
- 45 J. Glaser, A. S. Karas and S. C. Glotzer, *Journal of Chemical Physics*, 2015, **143**, year.
- 46 A. Rahman, *Phys. Rev.*, 1964, **136**, 405–411.
- 47 S. C. Glotzer, V. N. Novikov and T. B. Schröder, *The Journal of Chemical Physics*, 2000, **112**, 509.
- 48 G. Brambilla, D. El Masri, M. Pierno, L. Berthier, L. Cipelletti, G. Petekidis and a. B. Schofield, *Physical Review Letters*, 2009, **102**, 085703.
- 49 J. Mattsson, H. M. Wyss, A. Fernandez-Nieves, K. Miyazaki, Z. Hu, D. R. Reichman and D. A. Weitz, *Nature*, 2009, **462**, 83–86.
- 50 L. Berthier and G. Biroli, *Reviews of Modern Physics*, 2011, **83**, 587–645.
- 51 L. Berthier and T. a. Witten, *Physical Review E*, 2009, **80**, 021502.
- 52 T. E. Oliphant, *A guide to NumPy*, Trelgol Publishing, 2006.
- 53 R. Böhmer, K. L. Ngai, C. A. Angell and D. J. Plazek, *The Journal of Chemical Physics*, 1993, **99**, 4201–4209.
- 54 D. J. Plazek and K. L. Ngai, *Macromolecules*, 1991, **24**, 1222–1224.
- 55 M. M. Hurley and P. Harrowell, *Phys. Rev. E*, 1995, **52**, 1694.
- 56 M. T. Cicerone and M. D. Ediger, *The Journal of Chemical Physics*, 1995, **103**, 5684–5692.
- 57 W. Kob, C. Donati, S. Plimpton, P. Poole and S. Glotzer, *Physical Review Letters*, 1997, **79**, 2827–2830.
- 58 S. C. Glotzer, *Journal of Non-Crystalline Solids*, 2000, **274**, 342–355.
- 59 W. K. Kegel and A. van Blaaderen, *Science*, 2000, **287**, 290–293.
- 60 Z. Zhang, P. J. Yunker, P. Habdas and A. G. Yodh, *Physical Review Letters*, 2011, **107**, 1–5.
- 61 C. Donati, J. Douglas, W. Kob, S. Plimpton, P. Poole and S. Glotzer, *Physical Review Letters*, 1998, **80**, 2338–2341.
- 62 E. R. Weeks, J. C. Crocker, A. C. Levitt, A. Schofield and D. A. Weitz, *Science*, 2000, **287**, 627–631.
- 63 C. Donati, S. C. Glotzer, P. H. Poole, W. Kob and S. J. Plimpton, *Physical review. E, Statistical physics, plasmas, fluids, and related interdisciplinary topics*, 1999, **60**, 3107–3119.
- 64 P. Lucas, *Journal of Non-Crystalline Solids: X*, 2019, **4**, 100034.
- 65 S. Sastry and C. Austen Angell, *Nature Materials*, 2003, **2**, 739–743.
- 66 J. Geske, B. Drossel and M. Vogel, *AIP Advances*, 2016, **6**, year.
- 67 I. Kaori, M. CT and C. Angell, *Nature*, 1999, **398**, year.
- 68 A. Faraone, L. Liu, C. Y. Mou, C. W. Yen and S. H. Chen, *Journal of Chemical Physics*, 2004, **121**, 10843–10846.
- 69 M. Micoulaut, *Reports on Progress in Physics*, 2016, **79**, year.
- 70 W. S. Xu, Z. Y. Sun and L. J. An, *Soft Matter*, 2015, **11**, 627–634.
- 71 W. S. Xu, X. Duan, Z. Y. Sun and L. J. An, *Journal of Chemical Physics*, 2015, **142**, year.
- 72 A. Pal, V. A. Martinez, T. H. Ito, J. Arlt, J. J. Crassous, W. C. Poon and P. Schurtenberger, *Science Advances*, 2020, **6**, 1–10.
- 73 T. Vo and S. C. Glotzer, *Molecular Physics*, 2019, **117**, 3518–3526.
- 74 R. P. Sear, *Journal of Chemical Physics*, 2000, **113**, 4732–4739.
- 75 G. van Anders, D. Klotsa, N. K. Ahmed, M. Engel and S. C. Glotzer, *Proceedings of the National Academy of Sciences of the United States of America*, 2014, **111**, E4812–E4821.
- 76 I. Saika-Voivod, F. Smallenburg and F. Sciortino, *Journal of Chemical Physics*, 2013, **139**, year.
- 77 F. Smallenburg, L. Fillion and F. Sciortino, *Nature physics*, 2014, **10**, 653–657.
- 78 M. Singh, D. Dhabal, A. H. Nguyen, V. Molinero and C. Chakravarty, *Physical Review Letters*, 2014, **112**, 147801.
- 79 F. Smallenburg and F. Sciortino, *Physical Review Letters*, 2015, **115**, 1–5.
- 80 J. C. Lagarias and C. Zong, *Notices of the American Mathematical Society*, 2012, **59**, 1392.
- 81 M. D. Ediger, *Annu. Rev. Phys. Chem.*, 2000, **51**, 99–128.
- 82 E. R. Weeks, *ACS Macro Letters*, 2017, **6**, 27–34.
- 83 A. S. Karas, J. Dshemuchadse, G. Van Anders and S. C. Glotzer, *Soft Matter*, 2019, **15**, 5380–5389.
- 84 Y. Nagaoka, H. Zhu, D. Eggert and O. Chen, *Science*, 2018, **362**, 1396–1400.
- 85 Y. Nagaoka, R. Tan, R. Li, H. Zhu, D. Eggert, Y. A. Wu, Y. Liu, Z. Wang and O. Chen, *Nature*, 2018, **561**, 378–382.
- 86 K. Deng, Z. Luo, L. Tan and Z. Quan, *Chemical Society Reviews*, 2020, **49**, 6002–6038.



More tetrahedral particle shapes make less fragile hard particle glass-formers, as evidenced by the density-dependent slope of the log of relaxation time,  $s(\phi/\phi_c) \equiv \partial \log \tau_\alpha / \partial (\phi/\phi_c)$ .